INTERNATIONAL JOURNAL FOR NUMERICAL METHODS IN FLUIDS, VOL. 19, 1055–1081 (1994)

THREE-DIMENSIONAL MODELLING OF STEAM FLUSH FOR DNAPL SITE REMEDIATION

P. A. FORSYTH

Department of Computer Science, University of Waterloo, Waterloo, Ont. N2L 3G1, Canada

SUMMARY

Numerical simulation of steam flush for clean-up of non-aqueous phase liquid (NAPL) contaminated groundwater sites involves solution of the multiphase, multicomponent subsurface flow equations. This paper describes techniques for discretizing problems with horizontal wells in a three-dimensional tetrahedral mesh. The effectiveness of non-linear flux limiters for reducing numerical dispersion is discussed. Primary variable selection and thermodynamic state transition rules will also be compared. Some example results for several steam flush scenarios will be presented.

KEY WORDS Multiphase porous media flow Primary variable selection Horizontal wells

1. INTRODUCTION

Non-aqueous phase liquids (NAPLs) are a serious threat to groundwater supplies. Although NAPL exists primarily in the non-aqueous phase, small amounts of these contaminants dissolve in groundwater. Even these small concentrations can be very hazardous to human health. Since the amount of dissolved contaminant is very small, it may take many years (centuries) for a NAPL to dissolve sufficiently so that a free NAPL phase no longer exists. During this time an enormous plume of contaminated groundwater may develop. Consequently, current NAPL remediation strategies involve attempts to remove the source of the contaminant, the free NAPL phase itself.

Simple pumping methods will be incapable of removing the residual saturation of NAPLs. Typically, organic NAPL contaminants are volatile (e.g. gasoline, TCE, PCE). Consequently, injection of air into the contaminated zone will volatilize the NAPL. The contaminant-rich gas phase can then be removed by vacuum extraction.[1–6]

However, in the case of heterogeneous systems, or NAPL contaminants which are denser than water (DNAPLs), air injection may be ineffective. If air is injected below the water table (air sparging), then the gravitational effects will cause immediate upward movement of the gas phase and hence some of the NAPL phase may be bypassed. Similarly, heterogeneities may cause fingering of gas through low-permeability zones.

In these situations, applicaition of heat energy to the subsurface will increase the rate of vaporization of the NAPL phase. Heat is typically introduced by injecting steam below the contaminated zone.[7–9] Conductive heat transfer will help to ensure that contaminated zones which are bypassed by the convective fluid motion will also become heated. Recently, numerical methods for simulating steam injection for NAPL clean-up have been discussed in References 10–12. Two-dimensional problems were addressed in Reference 13.

The objective of this paper is to develop numerical methods for solution of a three-phase,

CCC 0271–2091/94/241055–27

Received 9 December 1993
Revised 10 May 1994

three-dimensional model of steam injection for NAPL remediation. The numerical problem is similar to thermal compositional reservoir simulation,[14–16] with the important added difficulty of allowing dispersive transport. Another important difference between contamination problems and reservoir simulation is that the NAPL contaminant is assumed to partition in the water phase. However, the solubility of NAPL contaminants in water is normally very small (i.e. the equilibrium mole fraction of NAPLs in water is about 10^{-4}–10^{-3} under standard conditions). In certain cases this causes some difficulty for the Newtonian iteration when phases appear and disappear. In this paper we will discuss primary variable selection and the phase transition rules for handling phase appearance and disappearance. Several different methods from those used previously[4,13,16] will be developed.

Methods for discretizing problems with horizontal wells in a tetrahedral mesh will be developed. A generalization of the methods used in References 17–20 will be employed.

In previous papers[4,3,21,22] the importance of positive transmissibilities and upstream weighting was discussed. Briefly, these methods ensure that, at convergence, quantities such as mole fractions and saturations are in the physical range (i.e. positive and less than one), regardless of grid size and time step size. Convergence (of the non-linear algebraic equations) to non-physical values (i.e. negative mole fractions) may cause the computation to abort.[13] In Reference 13 a method for perturbing the dispersion tensor so that positive transmissibilities resulted was developed. For model problems it was demonstrated[13] that his perturbation was $O(h)$, where h is the mesh size parameter. Consequently, this perturbation was the same size as the usual finite element discretization error and ensures convergence to the correct solution as the mesh size h goes to zero. However, positive mole fractions are obtained at all finite mesh sizes. This approach will be used in this work.

Owing to the highly non-linear nature of multiphase flow, upstream weighting for the mobilities is not a problem of great concern if one is interested primarily in total NAPL recovery, because of the self-sharpening behaviour of non-linear shocks.[23] However, it could be argued that upstream weighting of the mole fractions in the convective terms may lead to numerically diffused results at practical mesh sizes. The use of a non-linear flux limiter[24–27] for these terms will be introduced and compared with single-point upstream weighting.

In situations where rapid movement of the gas phase occurs, gas phase fingers may form which bypass the contaminated zone. The minimum width of a finger which can be resolved on any grid is the minimum internodal spacing. Consequently, there will be discretization errors introduced as a result of this effect. Some grid sensitivity studies of this effect will be presented for two-dimensional problems. Computational considerations preclude grid refinement studies in three dimensions.

Computations for a three-dimensional, heterogeneous remediation scenario will be presented. The effects of different placements of horizontal steam injectors and vertical production wells will be determined.

2. FORMULATION

The three phases considered are water (w), gas (g) and nonaqueous (n). The chemical components are water (w), air (a), NAPL component one (1) and NAPL component two (2). Assuming that chemical species $p = w, a, 1, 2$ can exist in any phase $l = g, w, n$ and all components are in instantaneous equilibrium, the conservation of mass for component p can be written as

$$\frac{\partial}{\partial t}\left(\sum_l (\phi S_l M_l X_{pl})\right) = -\sum_l \nabla\cdot(M_l X_{pl}\mathbf{V}_l) + \sum_l \nabla\cdot(\phi S_l \mathbf{D}_l M_l \nabla X_{pl}) + q_p \tag{1}$$

and the energy conservation equation is

$$\frac{\partial}{\partial t}\left(\sum_l (\phi S_l M_l U_l) + (1-\phi)U_r M_r\right) = -\sum_l \nabla\cdot(h_l M_l \mathbf{V}_l) + \sum_l \sum_p \nabla\cdot(\phi S_l \mathbf{D}_l M_l h_{pl} \nabla X_{pl}) + \nabla\cdot\beta\nabla T + q_{en}, \quad (2)$$

where the velocity of each phase l is given by

$$\mathbf{V}_l = -\mathbf{K}\cdot\lambda_l(\nabla P_l - \rho_l g \nabla D) \quad (3)$$

and where

S_l saturation of phase l
P_l pressure of phase l
M_l molar density of phase l
M_r molar density of rock r
ρ_l mass density of phase l
$\mathbf{K}$ absolute permeability tensor
λ_l k_{rl}/μ_l
μ_l viscosity of phase l
k_{rl} relative permeability of phase l
D depth
g gravitational acceleration
$\mathbf{D}_l$ dispersion/diffusion tensor for phase l
X_{pl} mole fraction of component p in phase l
q_p source/sink term for component p
T temperature
h_l enthalpy of phase l
h_{pl} enthalpy of component p in phase l
U_l internal energy of phase l
U_r internal energy of rock r
β heat conductivity of rock and fluids
q_{en} source/sink term for energy.

There exist the following constraints and constitutive relations among the above variables:

$$\begin{aligned} S_n + S_g + S_w &= 1, \\ P_g &= P_n + \alpha P_{cgn}(S_g) + (1-\alpha)[P_{cgw}(S_g) - P_{cnw}(S_w = 1)], \\ P_n &= P_w + \alpha P_{cnw}(S_w) + (1-\alpha)P_{cmw}(S_w = 1), \end{aligned} \quad (4)$$

where

$$\alpha = \min(1, S_n/S_n^*) \quad (5)$$

and P_{cgn}, P_{cnw} and P_{cgw} are experimentally determined capillary pressure curves, as are the relative permeabilities k_{rl}.[28] S_n^* is a blending parameter used to ensure that the capillary pressure has the correct form as the non-aqueous phase saturation goes to zero.[21] Although the pressure relations in equation (4) are more properly termed constitutive relations, we will refer to these

types of relations collectively as algebraic constraints, to distinguish them from the differential mass conservation equations.

In addition to the above equations, various phase equilibrium constraints must be satisfied. For example, for any phase l which is present,

$$\sum_p X_{pl} = 1. \tag{6}$$

Between any two phases i and j which exist, we assume phase partitioning (instantaneous equilibrium) of the form (for any component p)

$$X_{pi} = Z_{pij} X_{pj}, \tag{7}$$

where the Z_{pij} can be a function of any of the variables.

Although the above equations have been given for the most general case, we shall make some simplifying assumptions. The non-aqueous phase consists only of contaminants ($p = 1, 2$), the water phase contains a water component and both contaminants ($p = w, 1, 2$) and the gas phase can consist of all components ($p = a, w, 1, 2$). In other words,

$$\begin{aligned} X_{ai} &\equiv 0, \quad i = \mathrm{w}, \mathrm{n}, \\ X_{wi} &\equiv 0, \quad i = \mathrm{n}. \end{aligned} \tag{8}$$

Equations (1) and (2) represent five differential equations which can be used to determine five primary variables. All other (secondary) variables can be determined by means of the algebraic constraints, equations (4), (6) and (7). This will be discussed later.

3. PHYSICAL PROPERTIES

The physical properties such as densities, enthalpies, viscosities and so on are complex non-linear functions of temperature, mole fractions, pressure and saturations. Details of these correlations are given elsewhere.[13] As described in Reference 13, the thermal equilibrium ratios (equation (7)), latent heats and viscosities are exponential functions of temperature.

The dispersion/diffusion tensors have the form[2]

$$\phi S_l \mathbf{D}_l = \alpha_{\mathrm{T}}^l |\mathbf{V}_l| \mathbf{I} + (\alpha_{\mathrm{T}}^l - \alpha_{\mathrm{T}}^l) \frac{\mathbf{V}_l \mathbf{V}_l}{|\mathbf{V}_l|} + \phi S_l \tau d_l \mathbf{I}, \tag{9}$$

where α_{T}^l is the transverse dispersivity, α_{L}^l is the longitudinal dispersivity, d_l is the molecular diffusion coefficient (all in phase l) and τ is the tortuosity. Stone's second method is used for three-phase relative permeabilities.[28]

4. DISCRETIZATION

A control volume finite element approach is used to discretize equations (1) and (2). A Galerkin finite element method is used for the transport terms and an influence coefficient method is used to handle the non-linearities.[29] Upstream weighting is used for the mobilities ($\lambda_l = k_{rl}/\mu_l$). Upstream-weighted mobilities can be shown to converge to the physically correct solution for multiphase flow situations[30] with countercurrent gravitational flow. The time derivative terms are discretized using mass lumping and backward Euler time stepping. Further details about this method can be found in References 4, 21 and 22.

If N_i are the usual Lagrange polynomial C^0 basis functions, where

$$\begin{aligned} N_i &= \begin{cases} 1 & \text{at node } i, \\ 0 & \text{at all other nodes,} \end{cases} \\ \sum_j N_j &= 1 \quad \text{everywhere in the solution domain,} \end{aligned} \tag{10}$$

and if

$$\begin{aligned} P_l &= \sum_j P_{lj} N_j, \\ \psi_l &= \sum_j \psi_{lj} N_j = \sum_j (P_{lj} - \rho_{lj} g D_j) N_j, \\ S_l &= \sum_j S_{lj} N_j, \\ T &= \sum_j T_j N_j, \\ X_{pl} &= \sum_j X_{plj} N_j, \end{aligned} \tag{11}$$

then the final discrete equation for conservation of component p is

$$\begin{aligned} &\left[\left(\sum_l (\phi S_l M_l X_{pl})\right)_i^{N+1} - \left(\sum_l (\phi S_l M_l X_{pl})\right)_i^{N}\right] \frac{V_i}{\Delta t} = \sum_l \sum_{j \in \eta_i} (M_l \lambda_l)^{N+1}_{\mathrm{ups}(i,j)} (X^*_{pl})^{N+1}_{\mathrm{vl}(i,j)} \gamma_{ij} (\psi_{lj}^{N+1} - \psi_{li}^{N+1}) \\ &\quad + \sum_l \sum_{j \in \eta_i'} (M_l)^{N+1}_{ij+1/2} (\gamma'_{ij})^M_l (X_{plj}^{N+1} - X_{pli}^{N+1}) + (q_p)_i^{N+1} V_i \end{aligned} \tag{12}$$

and the discrete energy conservation equation is

$$\begin{aligned} &\left[\left(\sum_l [\phi S_l M_l U_l + (1-\phi) U_r M_r]\right)_i^{N+1} - \left(\sum_l [\phi S_l M_l U_l + (1-\phi) U_r M_r]\right)_i^{N}\right] \frac{V_i}{\Delta t} \\ &\quad = \sum_l \sum_{j \in \eta_i} (M_l \lambda_l h_l)^{N+1}_{\mathrm{ups}(i,j)} \gamma_{ij} (\psi_{lj}^{N+1} - \psi_{li}^{N+1}) + \sum_l \sum_p \sum_{j \in \eta_i'} (M_l h_{pl})^{N+1}_{ij+1/2} (\gamma'_{ij})^M_l (X_{plj}^{N+1} - X_{pli}^{N+1}) \\ &\quad + \sum_{j \in \eta_i''} \gamma''_{ij} (T_j^{N+1} - T_i^{N+1}) + (q_{\mathrm{en}})_i^{N+1} V_i, \end{aligned} \tag{13}$$

where

$$\begin{aligned} V_i &= \int_v N_i \, \mathrm{d}v, \\ \psi_{li}^{N+1} &= P_{li}^{N+1} - \rho_{l,ij+1/2}^{N+1} g D_i, \\ \rho_{l,ij+1/2} &= (\rho_{l,i} + \rho_{l,j})/2, \\ (M_{l\ldots})_{ij+1/2} &= (M_{li\ldots} + M_{lj\ldots})/2, \\ (M_l \lambda_{l\ldots})_{\mathrm{ups}(i,j)} &= \begin{cases} (M_l \lambda_{l\ldots})_i^{N+1} & \text{if } \gamma_{ij}(\psi_{lj}^{N+1} - \psi_{li}^{N+1}) < 0, \\ (M_l \lambda_{l\ldots})_j^{N+1} & \text{if } \gamma_{ij}(\psi_{lj}^{N+1} - \psi_{li}^{N+1}) > 0, \end{cases} \end{aligned} \tag{14}$$

$(X^*_{pl})_{\mathrm{vl}(i,j)}$ is the van Leer weighting and the γ_{ij} are given by

$$\gamma_{ij} = -\int_v \nabla N_i \cdot \mathbf{K} \cdot \nabla N_j \, \mathrm{d}v,$$

$$(\gamma'_{ij})^M_l = -(S_l)^{N+1}_{ij+1/2} \int_v \nabla N_i \cdot \left(\frac{\phi S_l \mathbf{D}_l}{S_l}\right)^N \cdot \nabla N_j \, \mathrm{d}v, \tag{15}$$

$$\gamma''_{ij} = -\int_v \nabla N_i \cdot \beta \cdot \nabla N_j \, \mathrm{d}v.$$

Here η_i, η'_i and η''_i are the set of neighbour nodes of node i such that γ_{ij}, γ'_{ij} and γ''_{ij} are non-zero. Note that the mobility term $M_l\lambda_l$ in equations (12) and (13) is always upstream-weighted, while the mole fraction term in the convective transport term is flux-limited.

Linear triangular elements are used in two dimensions and tetrahedral linear elements are used for three-dimensional problems. As discussed in References 4, 13, 21 and 22, it is desirable that γ_{ij} and γ'_{ij} should be non-negative. The requirement that $\gamma_{ij} \geqslant 0$ ensures that the discrete fluid flux is in the physically correct direction. This amounts to a condition on the type of mesh which can be used.[21,22] In this work simple grids will be used which will ensure that $\gamma_{ij} > 0$ always holds. In general it is not possible to ensure that both $\gamma_{ij} \geqslant 0$ and $\gamma'_{ij} \geqslant 0$. If $\gamma'_{ij} < 0$, then negative mole fractions can be a converged solution of the discrete equations at finite mesh sizes.[4] However, as discussed in Reference 13, it is possible to perturb the dispersion tensor so that only non-negative mole fractions are solutions to the discrete algebraic equations. This perturbation can be shown (at least for a simple case) to cause only an $O(h)$ error in the solution, where h is the mesh size parameter.[13] This method will be used in the following.

The discrete equations (12) and (13) are solved using full Newton iteration. The Jacobian is solved using an incomplete and LU factorization[31] with CGSTAB acceleration.[32]

In order to avoid non-physical movement of negative mass into a node, X^*_{pl} in equation (12) is defined as

$$X^*_{pl} = \max(0, X_{pl}). \tag{16}$$

To avoid problems with the Newton iteration, the function in equation (16) is actually smoothed at points of discontinuous derivative. In equation (15) $(S_l)_{ij+1/2}$ is given by

$$(S_l)_{ij+1/2} = \frac{2S_{li}S_{lj}}{S_{li} + S_{lj}}. \tag{17}$$

The form of the source/sink terms in equations (12) and (13) is such that[21]

$$(q_p)_i \equiv 0 \quad \text{if } X_p \leqslant 0, \tag{18}$$

so that mass withdrawal from a node goes to zero as the mole fraction goes to zero. Equations (12) and (13) are fully implicit except for the dispersion tensor in equation (15).

The van Leer weighting in equation (14) is defined by

$$(X^*_{pl})_{\mathrm{vl}(i,j)} = (X^*_{pl})_{\mathrm{ups}(i,j)} + \sigma(r_{ij})\left(\frac{X^*_{\mathrm{dwn}(i,j)} - X^*_{\mathrm{ups}(i,j)}}{2}\right), \tag{19}$$

where $X^*_{\mathrm{dwn}(i,j)}$ is the downstream point between nodes i and j:

$$\mathrm{dwn}(i,j) = i + j - \mathrm{ups}(i,j), \tag{20}$$

The smoothness sensor r_{ij} in equation (19) is defined by

$$r_{ij} = \begin{cases} \dfrac{(X^*_{pl})_i - (X^*_{pl})_{i2up(l,i)}}{(X^*_{pl})_j - (X^*_{pl})_i} & \text{if } i = \text{ups}(i,j), \\ \dfrac{(X^*_{pl})_j - (X^*_{pl})_{i2up(l,j)}}{(X^*_{pl})_i - (X^*_{pl})_j} & \text{if } j = \text{ups}(i,j), \end{cases} \tag{21}$$

where $i2up(l, i)$ is given by

$$i2up(l, i) = j^* \quad \text{such that } \Psi(l, j^*) = \max_{j \in \eta_i} \Psi(l, j), \tag{22}$$

with

$$\Psi(l, j) = \max(0, (M_l \lambda_l)^{N+1}_{ups(i,j)} \gamma_{ij} (\psi^{N+1}_{lj} - \psi^{N+1}_{li})). \tag{23}$$

In equation (19) a van Leer limiter[24,25] is used:

$$\sigma(r) = \begin{cases} 0 & \text{if } r \leqslant 0, \\ 2r/(1+r) & \text{if } r > 0. \end{cases} \tag{24}$$

For one-dimensional, single-phase, incompressible flow $i2up(l, i)$ would be the phase second point upstream and equations (19)–(24) would result in a TVD scheme.[25] The use of the TVD method with a non-linear flux limiter has been shown (at least for model problems) to give high-resolution, oscillation-free solutions.[25] Flux limiters have been used for the mobilities in petroleum reservoir simulation.[26] However, it is our experience that, in terms of total NAPL mass removal, numerical diffusion of the saturation shock front is not particularly serious owing to the highly non-linear (self-sharpening) nature of the shock. For problems which are almost single-phase and constant velocity, where the NAPL phase is non-existent, the contaminant transport equations (12) reduce to the linear advection–dispersion equation. In this case upstream weighting of the mole fractions may cause excessive false diffusion.

In two or more dimensions it is known that, in the case of scalar hyperbolic conservation laws, any TVD scheme is at most first-order-accurate (i.e. upstream weighting).[34] Consequently, use of flux-limiting schemes in two or more dimensions is based on analogies to one-dimensional flows rather than rigorous argument.

In two or more dimensions it is possible to define the second upstream point ($i2up$ in equation (22)) as the second point upstream of the interface along the grid line. We will refer to this definition of the second upstream point as the geometric second upstream point. This geometric definition of the second upstream point is inappropriate for heterogeneous subsurface flow problems. To see this, consider a node i which is adjacent to a node $i2up$. Suppose node $i2up$ has a very small, or zero, absolute permeability. If node i is upstream of a node j, then node $i2up$ is the geometric second upstream point to node j. Clearly, in this situation node $i2up$ should have no influence on the flow in node j.

To avoid these problems, equation (22) attempts to select the second upstream point by going back along the streamline from the upstream point.[35] The second upstream point is always a node location. It is possible to attempt to interpolate the value of the second upstream point, but this is a dubious proposition for heterogeneous media. For further justification of this choice of the second upstream point the reader is referred to Reference 35.

Note that the definition (21) for the smoothness sensor[33] assumes that the phase velocity along the streamline is approximately constant. If flux limiting is applied to the non-linear

mobility terms (λ_l) in equations (12) and (13), it is possible to use the flux function as the smoothness detector.[26] However, in Reference 33 various forms of smoothness detector are used for true two-dimensional situations, not just the flux functions, with apparently good results.

It is important to note that flux limiters based on TVD arguments cannot be guaranteed to be oscillation-free in two or more dimensions.[34] Our initial experiments with flux limiters often caused the simulation to abort owing to too small time steps. This problem was traced to the spurious appearance and disappearance of phases with the flux limiter (this will be discussed in the next section). Consequently, we ended up using the flux limiter equation (21) in regions where the flow was virtually linear (i.e. the saturations are slowly changing). In this case the assumption that the phase velocity is nearly constant along a streamline is reasonable, which gives the simple and compact scheme (21).

Note that different weighting methods for the mole fraction terms and for the mobility terms have also been used in Reference 36. A two-point upstream method (without constraints) and a third-order method were used in Reference 36. However, these methods are not guaranteed to be monotone even for one-dimensional flows.

5. PHASE APPEARANCE AND DISAPPEARANCE

The primary variables for a node are those which are regarded as independent when constructing the Jacobian. The choice of primary variables can greatly influence the convergence of the Newton iteration.[37] In the case of a non-condensable gas (e.g. air), if the mole fractions are taken as primary variables, then problems arise in handling cases where the gas phase appears and disappears owing to air transport.[38]

One way of circumventing this problem is to assume that a small amount of air dissolves in the water phase. This method was used for gas-venting simulations as described in Reference 4. However, as discussed in Reference 13, this technique resulted in poor convergence of the Newton iteration for two-dimensional steam flush problems.

A comparatively simple solution to this problem[13] is to assume that a small amount (e.g. $S_g = 10^{-4}$) of the gas phase is always present. This results in the set of states and transition rules discussed below. The four states (Method 1) are

$$
\begin{array}{ll}
\textit{State 1} & \text{Assumptions: all phases present} \\
 & \text{Primary variables: } P_n,\ T,\ S_n,\ S_w,\ X_{1n} \\
\textit{State 2} & \text{Assumptions: } S_n \equiv 0,\ S_w > 0,\ S_g > 0 \\
 & \text{Primary variables: } P_n,\ T,\ S_w,\ X_{1g},\ X_{2g} \\
\textit{State 3} & \text{Assumptions: } S_n \equiv 0,\ S_w \equiv 0,\ S_g \equiv 1 \\
 & \text{Primary variables: } P_n,\ T,\ X_{1g},\ X_{2g},\ X_{wg} \\
\textit{State 4} & \text{Assumptions: } S_w \equiv 0,\ S_n > 0,\ S_g > 0 \\
 & \text{Primary variables: } P_n,\ T,\ S_n,\ X_{1n},\ X_{wg}
\end{array}
\tag{25}
$$

with the transition rules

```
if (state = 1) then
    if (S_w < 0) then
        state := 4
    elseif (S_n < 0) then
        state := 2
    endif
```

```
elseif (state = 2) then
    if (S_w < 0) then
        state := 3
    elseif (∑_p X_pn > 1) then
        state := 1
    endif
elseif (state = 3) then
    if (∑_p X_pn > 1) then
        state := 4
    elseif (∑_p X_pw > 1) then
        state := 2
    endif
elseif (state = 4) then
    if (S_n < 0) then
        state := 3
    elseif (∑_p X_pw > 1) then
        state := 1
    endif
endif
```

(26)

This set of discrete equations admits a possible non-physical solution[13] with

$$S_g^{N+1} \sim -|\varepsilon|, \tag{27}$$

$$X_{ag}^{N+1} < 0. \tag{28}$$

In order to avoid this non-physical solution, a penalty source term is added to the air conservation equation:

$$q_a^* V_i = \begin{cases} (X_{ag})^2 \max(\phi S_n M_n, \phi S_w M_w) V_i / \Delta t & \text{if } S_g < 0 \text{ and } X_{ag} < 0, \\ 0 & \text{otherwise.} \end{cases} \tag{29}$$

The reader is referred to References 13 and 38 for more details about the penalty source (29).

In some situations we have observed that the set of states and primary variables of (25) has poor convergence behaviour for the Newton iteration. This seems to occur when large amounts

Table I. Conversion rules for producing new states in Method 2 from states in Method 1

Method 1	Conversion rule	Method 2
State 1	$(X_{ag}$ or $S_g) > \varepsilon_1$; $S_g > 0$	State 8
State 1	$(X_{ag}$ and $S_g) < \varepsilon_1$; $S_g > 0$	State 1
State 1	$S_g \equiv 0$	State 5
State 2	$(X_{ag}$ or $S_g) > \varepsilon_1$; $S_g > 0$	State 9
State 2	$(X_{ag}$ and $S_g) < \varepsilon_1$; $S_g > 0$	State 2
State 2	$S_g \equiv 0$	State 6
State 3	No change	State 3
State 4	$(X_{ag}$ or $S_g) > \varepsilon_1$; $S_g > 0$	State 10
State 4	$(X_{ag}$ and $S_g) < \varepsilon_1$; $S_g > 0$	State 4
State 4	$S_g \equiv 0$	State 7

of water are flushed past a NAPL contaminant below the water table. In this case the Newton iteration oscillates when the mole fraction of contaminant approaches zero. This problem appears to be due to the small amount of gas phase saturation which is required in Method 1 below the water table. Consequently, we can attempt to alleviate this problem by using a set of states which allows the gas phase to disappear completely. This alternative approach uses the following set of states and primary variables (Method 2):

State 1	Assumptions: all phases present; X_{ag} and $S_g \ll \varepsilon_1$	
	Primary variables: P_n, T, S_n, S_w, $(X_{ag}S_g)$	
State 2	Assumptions: $S_n \equiv 0$, $S_g > 0$, $S_w > 0$; X_{ag} and $S_g \ll \varepsilon_1$	
	Primary variables: P_n, T, S_n, X_{1g}, $(X_{ag}S_g)$	
State 3	Assumptions: $S_n \equiv 0$, $S_g \equiv 1$, $S_w \equiv 0$	
	Primary variables: P_n, T, X_{1g}, X_{2g}, X_{wg}	
State 4	Assumptions: $S_n > 0$, $S_g > 0$, $S_w \equiv 0$; X_{ag} and $S_g \ll \varepsilon_1$	
	Primary variables: P_n, T, S_n, X_{1n}, $(X_{ag}S_g)$	
State 5	Assumptions: $S_n > 0$, $S_g \equiv 0$, $S_w > 0$	
	Primary variables: P_n, T, S_w, X_{1g}, $(X_{ag}S_g)$	(30)
State 6	Assumptions: $S_n \equiv 0$, $S_g \equiv 0$, $S_w \equiv 1$	
	Primary variables: P_n, T, X_{1w}, X_{ww}, $(X_{ag}S_g)$	
State 7	Assumptions: $S_n \equiv 1$, $S_g \equiv 0$, $S_w \equiv 0$	
	Primary variables: P_n, T, X_{1n}, $(X_{ww}S_w)$, $X_{ag}S_g)$	
State 8	Assumptions: all phases present; X_{ag} or $S_g > \varepsilon_1$	
	Primary variables: P_n, T, S_n, S_w, X_{1n}	
State 9	Assumptions: $S_n \equiv 0$, $S_g > 0$, $S_w > 0$; X_{ag} or $S_g > \varepsilon_1$	
	Primary variables: P_n, T, S_w, X_{1g}, X_{2g}	
State 10	Assumptions: $S_n > 0$, $S_g > 0$, $S_w \equiv 0$; X_{ag} or $S_g > \varepsilon_1$	
	Primary variables: P_n, T, S_n, X_{1n}, X_{wg}	

In order to understand how the states in Method 2 were derived from Method 1, Table I gives a list of the states in Method 1 and the circumstances (or conversion rules) for generating the states in Method 2.

Note that States (1, 2, 4, 5, 6, 7) in (30) use products of a mole fraction and a saturation as a primary variable. This can be thought of as analogous to the use of global mole fractions as primary variables, which is sometimes used in compositional reservoir simulation.[15,16] In fact, the product $(x_{ag}S_g)$ is essentially the global mole fraction for the air component if it is multiplied by the gas density and divided by the total molar density. The use of the product-type primary variables in (30) permits easy computation of the other secondary variables and does not require an inner iteration in the flash calculation as does the global mole fraction formulation.[15]

States 1, 2, 4 are present only to avoid pathological situations where $S_g > 0$ and both S_g and X_{ag} are very small, since the Jacobian becomes singular in the limit as both S_g, $X_{ag} \to 0$ if S_g and X_{ag} are primary variables. In practice, we use a value of $\varepsilon_1 = 10^{-5}$ in (30), so that typically these states are rarely used.

In fact, it is possible to use States 1, 2, 4 for all cases where $S_g > 0$, and not use States 8, 9, 10. However, initial tests showed poor convergence with this set of primary variables. This may be because the secondary variable computation requires division by a (possibly) small value, which is always a dangerous procedure.

We will not try the reader's patience at this point with a complete set of transition rules for all the states in the primary variable set (30) (Method 2). Suffice to say, these rules are analogous

to (26). The state-switching criteria are based on the appearance of negative saturations or $\sum_p X_{pl} > 1$ for any phase l which is not present. Since the Jacobian is constructed numerically, the addition of different states and transition rules is not a particularly difficult coding task.[39] As described in References 39 and 40, the differentials in the Jacobian are approximated by numerical differencing. Owing to the mass conservative nature of the discrete equations, the Jacobian can be constructed very efficiently.[39,40]

Since the flux-limiting scheme (19–24) is not guaranteed to be oscillation-free in two or more dimensions, this approach can be dangerous to use in regions where the problem is highly non-linear. If a non-trivial negative mole fraction is the converged solution to the discrete equations, this can cause tremendous difficulties.[13] Consequently, the flux limiter in equations (19)–(24) will be applied only to the contaminant mole fractions ($p = 1, 2$). Additionally, the flux limiter is used for the flux between node i and mode j only if

```
if (∑_p X_pnk < tol; ∀k ∈ η_i ∪ η_j) then
    use flux limiter
else                                                    (31)
    use upstream weighting
endif
```

The constraint (31) ensures that flux limiting is only used for nodes which are not neighbours of any nodes where an NAPL phase is likely to appear. Initial tests without the constraint (31) sometimes caused very poor convergence of the Newton iteration. This was traced to the fact that the flux limiter sometimes caused small oscillations in the mole fractions. This in turn sometimes caused spurious state changes in nodes where the NAPL phase was close to appearing or had just disappeared. Typically, a value of tol = 0·5 in (31) prevents a poor convergence behaviour for the Newton iteration.

Note that (31) effectively precludes use of the flux limiter in regions where $S_n > 0$. Since we are attempting to simulate processes for removing NAPLs from the subsurface by injection of steam, a properly designed process will cause rapid vaporization of the NAPL phase. Unfortunately, use of the flux limiter at any node with $S_n > 0$ virtually always caused problems. Consequently, use of (31) restricts the application of the flux limiter to nodes far away from the free NAPL zone, where the flow is almost linear.

6. MODELLING OF HORIZONTAL WELLS

Horizontal wells are now popular methods for increasing oil recovery in petroleum reservoirs.[19] New drilling technology has reduced the cost of drilling shallow horizontal wells, and prototype field-scale experiments have been carried out using this technology for sursurface remediation problems.

Horizontal wells cannot, by their very nature, be regarded as simply collections of decoupled nodal source/sink terms. For example, a given quantity of steam will be injected into the well. However, the amount of steam which will actually enter each node along the wellbore length will depend on that node's pressure. Only the total amount injected at all nodes is known *a priori*. In more complex situations the well may backflow. In other words, even though the total fluid flow is from the well into the formation, there may be some nodes where the flow is actually from the formation into the well.

A simple method to model these wells is to create a virtual node or cell having the volume of the actual wellbore. The values of the fluid saturations, viscosities and so on can be regarded

as average properties of the fluid in the wellbore. The pressure in this virtual node is deemed to be at some arbitrary point in the wellbore. Pressures at any other point along the wellbore are computed by using the wellbore fluid density to compute the fluid head.[19] Similar ideas have been advocated for use in petroleum reservoir simulation.[20] It is possible to actually model the flow along the wellbore using two-phase pipe flow correlations, but this does not appear to result in any significant change in the simulation results.[19]

Consequently, this virtual wellbore node can be treated just like any other node, since the form of the discrete equations for this node is the same as for any other node, with the exception that some of the fluid properties are different (e.g. relative permeabilities for this node are straight lines). Conceptually, we can imagine that this virtual node overlays all the nodes in the mesh which are along the wellbore.

It remains then to specify the flow terms between the wellbore node and a mesh node. Consider the mass flow equation for component p at node i (equation (12)). Assuming that there is no dispersive flux between wellbore node v and node i, the mass flux of component p will be given by

$$\text{mass flux} = \sum_l (M_l \lambda_l)^{N+1}_{\text{ups}(i,v)} (X^*_{pl})^{N+1}_{\text{ups}(i,v)} \gamma_{iv} (\psi^{N+1}_{iv} - \psi^{N+1}_{li}). \tag{32}$$

The term $(\psi_{lv} - \psi_{li})$ in equation (32) is given by

$$(\psi_{lv} - \psi_{li}) = P_{lv} - P_{lj} - \rho_v g(D_v - D_i). \tag{33}$$

If the mesh size is such that the mesh size in a direction perpendicular to the wellbore is of the same size as the actual wellbore radius, then γ_{iv} in equation (32) is simply set to a large number to force the node pressure to be equal to the wellbore pressure. More typically, the mesh spacing is large compared with the wellbore radius. Assuming that the flow is radial near the wellbore, then the methods of Reference 41 can be used to determine γ_{iv}. For simplicity we assume that the permeability tensor is diagonal,

$$\mathbf{K} = \begin{pmatrix} k_x & 0 & 0 \\ 0 & k_y & 0 \\ 0 & 0 & k_z \end{pmatrix}, \tag{34}$$

and that the wellbore is along the x-axis. In this case the final expression for γ_{iv} is

$$\begin{aligned}
\gamma_{iv} &= \frac{2\pi k' h_i \sum_{j \in \eta'_i, j \neq v} \gamma_{ij}}{\sum_{j \in \eta'_i, j \neq v} \gamma_{ij} \log(r'_j / r'_w) - 2\pi k' h_i}, \\
r'_w &= \frac{r_w}{2} \left[\left(\frac{k_y}{k_z} \right)^{1/4} + \left(\frac{k_z}{k_y} \right)^{1/4} \right], \\
r'_j &= \left(\frac{z_j^2 k'}{k_z} + \frac{y_j^2 k'}{k_y} \right)^{1/2}, \\
k' &= (k_z k_y)^{1/2}, \\
h_i &= \frac{\|\mathbf{x}_i - \mathbf{x}_\alpha\|}{2} + \frac{\|\mathbf{x}_i - \mathbf{x}_\beta\|}{2},
\end{aligned} \tag{35}$$

where r_w is the actual wellbore radius, x_j and y_j are the x- and y-coordinates of node j respectively, η_i' are those neighbour nodes of node i which are not along the wellbore direction and α and β are neighbours of node i along the wellbore. The above expression is a three-dimensional generalization of the expressions given in Reference 18. Note that there appears to be a typographical error in the two-dimensional result given in Reference 18. For further details the reader is referred to References 41 and 42.

Since the wellbore pseudonode has a small volume compared with surrounding nodes, it might be expected that this could cause problems for the Newton iteration if the wellbore saturations or mole fractions change suddenly. During some stress testing of this wellbore formulation we were able to take reasonable time step sizes if we multiplied the wellbore volume by a factor of ~ 100. This effectively increased the time scale of the wellbore node.[20] Cumulative production graphs (with the increased wellbore node volume) were virtually identical with the graphs obtained using the actual wellbore volume. However, in all our remediation scenarios it was unnecessary to increase the wellbore pseudonode volume. For injection wells which did not backflow, the wellbore node rapidly becomes saturated with the injected fluid and then the saturations of the wellbore node stay constant. A properly placed production well produced mostly gas and some water, which also resulted in only a slow change in production wellbore node saturations. Nevertheless, there may be some cases where the Newton iteration convergence can be enhanced by increasing the size of the effective volume of the wellbore pseudonode. It would appear that this can be done without significantly altering the computational results.

7. EFFECTIVENESS OF THE NON-LINEAR FLUX LIMITER

Recall that the flux limiter (20)–(24), (31) was designed to reduce dispersion in situations where the contaminant motion was essentially determined by a linear transport process (i.e. far away from regions where $S_n > 0$).

Figure 1 shows a two-dimensional areal example (no gravity). No-flow boundaries are used on all edges of the domain. NAPLs and air are injected at the upper left corner and a constant pressure producer is placed at the lower right corner. This is a true multidimensional situation, since the flow is first diverging near the injector and then converges near the producer. All dispersion terms in equation (1) were set to zero, isothermal flow was simulated and a single

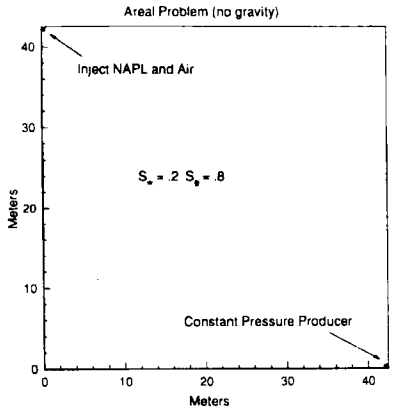

Figure 1. Areal test problem for comparison of single-point upstream and non-linear flux limiter methods

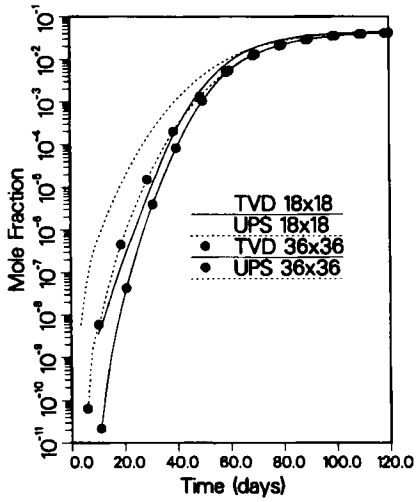

Figure 2. NAPL mole fraction in gas phase at producer for non-linear flux limiter (TVD) and single point upstream (UPS) methods

NAPL component was injected. The injection rate of air was quite large so that a free NAPL phase ($S_n > 0$) appeared in only a few nodes near the injector. The rapid air motion caused the NAPL to volatilize. The NAPL contaminant was then transported in the gas phase to the producer.

Figure 2 shows the results for the NAPL mole fraction in the gas phase at the producer using both single-point upstream (UPS) and non-linear flux limiter (TVD) methods for both 18 × 18 and 36 × 36 grids. Note that the non-linear flux limiter does show some improvement over the single-point upstream method (i.e. a steeper rise in the mole fraction) and appears to be converging faster (as the grid is refined) than the single-point upstream weighting. This is especially noticeable at very small mole fractions (note the log scale used in Figure 2), which is important for determining safe drinking water levels of contamination.

Consequently, all runs reported in the following will use the non-linear flux limiter (20)–(24) with the constraint (31).

8. CHOICE OF PRIMARY VARIABLES

Two-dimensional computational results using the primary variable set (25) (Method 1) were reported in Reference 13. Recall that it is necessary to use the penalty source (29) with this primary variable set to ensure convergence to physical solutions. Although this primary variable set worked well generally, there were some situations where poor convergence of the Newton iteration was noted.

Figure 3 shows a two-dimensional cross-section. No-flow boundaries are imposed on the upper and lower surfaces. Hydrostatic pressure was imposed on the left and right boundaries (with the pressures at the points noted in Figure 3), which resulted in a sloping water table and groundwater flow as shown.

The isothermal test problem used the following injection scenario. The system was allowed to equilibrate for 7 days, then a small amount of single-component DNAPL was injected during the period from 7 to 7·1 days. The computation was then continued to 100 days. The DNAPL

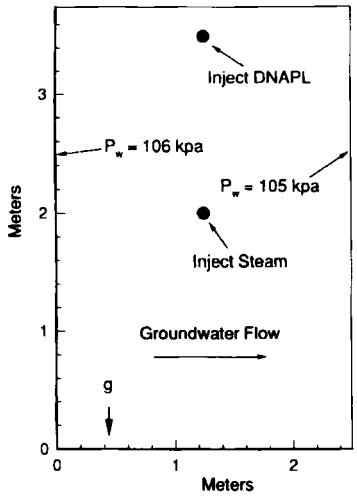

Figure 3. Two-dimensional cross-section for test of primary variable sets

first sinks below the water table and then dissolves into the water phase. Transport also occurs in the gas phase (a dense gas plume sinks down along the top of the water table.) A 10 × 15 grid was used.

This problem was solved with both the primary variable set (25) (Method 1) and the set (30) (Method 2). Table II gives the total number of Newton iterations required for both methods (isothermal problem).

Although the computed solutions at 100 days for both methods were very similar, the number of Newton iterations for the primary variable set (25) (Method 1) was about 2·4 times the number of Newton iterations for the primary variable set (30) (Method 2). Close examination of the Newton iterations for Method 1 revealed the following pattern: nodes below the water table, which had small NAPL saturations, would switch to a state with no NAPL saturation (owing to dissolution in the passing water phase). The actual switch to a state with no NAPL did not appear to cause any problems. However, in subsequent time steps the amount of NAPL dissolved in the water phase would rapidly decrease to a very small value. During the course of the Newton iteration the mole fraction of NAPL in the water phase would overshoot to a negative value and the iteration would never recover. This would cause a repeat time step. Various methods were tried to alleviate this problem (e.g. heavy underrelaxation, modification of non-physical densities for negative mole fractions, etc.) without success. Possibly this problem

Table II. Computational efficiency for Methods 1 and 2

	Total Newton iterations*	
	Isothermal problem	Steam injection
Method 1	599	609
Method 2	247	669

* CPU time proportional to Newton iteration count.

is due to the small gas saturation, which is required for this formulation, below the water table.

However, as seen in Table II, this problem was entirely absent from the computation using the primary variable set of Method 2. As noted in previous studies, the choice of primary variables can often have a dramatic effect on the convergence of the Newton iteration.[37]

The above test problem was converted into a steam injection problem by following the same DNAPL injection procedure until 7·1 days. Then high-temperature steam was injected at the point shown in Figure 3 during the period from 7·1 to 7·6 days. The injection rate was such as to cause the NAPL to volatilize, then be convected in the gas phase to the cool boundary regions and finally to condense (the boundaries were maintained at 293 K). Subsequently, cold water was injected (at the former steam injection point) during the period from 7·6 to 7·9 days, which caused the entire steam zone to collapse. This problem constituted a very severe test, since many state switches were triggered.

Although exact converged solutions of the discrete equations using the primary variables of (30) must have positive mole fractions and saturations, rather surprisingly, we found that convergence was enhanced considerably by addition of the penalty source equation (29). In fact, without the penalty source some example runs using Method 2 would converge to small negative air mole fractions (within the convergence tolerance). This negative air mole fraction would accumulate from time step to time step and eventually cause problems. Use of the penalty source eliminated this problem. Consequently, the penalty source was used for both the primary variable sets (26) and (30). It is also our understanding that convergence of a global mole fraction formulation of this problem was also enhanced by the use of a similar penalty source.[43]

The total Newton iterations for Methods 1 and 2 for this problem (steam injection) are compared in Table II. In this case Method 1 is actually slightly more efficient than Method 2. Analysis of the Newton iterations showed that Method 2 generally required an extra iteration after switching the gas phase on or off, compared with Method 1. Since the gas phase in Method 1 is always present, Method 1 does not require these extra iterations.

Consequently, for pure steam injection problems there does not appear to be any advantage to using the primary variable set of Method 2; thus Method 1 will be used for all subsequent steam injection computations.

However, the performance penalty for using Method 2 compared with Method 1 is small and in some circumstances (the isothermal problem) Method 2 greatly outperforms Method 1. Therefore for general multiphase, multicomponent simulation we would recommend Method 2 be used.

9. A TWO-DIMENSIONAL EXAMPLE

Since it is impractical to carry out a grid refinement study for a full three-dimensional problem (the 3-D problems presented in the next section require about 30–40 h of CPU time on an R-6000 workstation), we will consider a two-dimensional cross-sectional problem and carry out this computation on two different grid sizes. This two-dimensional cross-section is then converted into a full three-dimensional problem. It can be reasonably argued that the discretization error observed in the two-dimensional case is about the same size as the error in the full three-dimensional problem. As pointed out in Section 1, the minimum gas finger width which can be resolved on any grid is of the order of the size of the node spacing. This discretization effect is noticeable on the two-dimensional cross-section (as will be seen) but does not have much effect on the total contaminant recovery. Although it can reasonably be assumed that this will be true for a three dimensional simulation using a grid size comparable with the two-dimensional

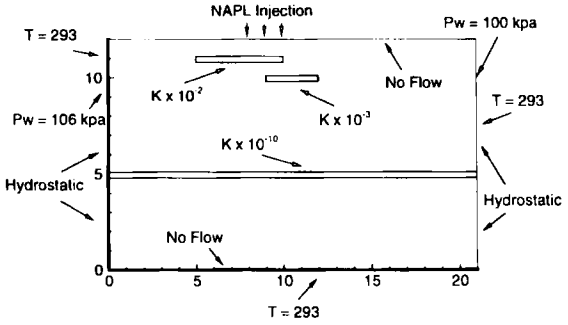

Figure 4. Two dimensional DNAPL steam injection cross-section

cross-section, we are unable to confirm this with the computational resources at our disposal. It is possible that the discretization error for the three-dimensional fingers is very different from that for two-dimensional fingers.

Figure 4 shows the geometry for this example. The absolute permeabilities were 10^{-12} m^2 everywhere except for the low-permeability barriers shown. The cross-section is 4 m thick. Note that there is an impermeable layer at $z = 5$ m. Since the computational domain is extended into the region below this impermeable layer, this will simulate heat loss below the steam injector. Both left and right boundaries are held at a constant temperature (293 K) and hydrostatic pressure is maintained with pressure fixed at the points noted in Figure 4. This causes cold groundwater flow from left to right, with a sloping water table 1–2 m below the surface. No heat loss or fluid flow is permitted through the upper surface.

The system is first allowed to equilibrate for 50 days and then a mixture of TCE and toluene (50% each by volume) is injected at a rate of 0·05 m^3 day^{-1} during the period from 50 to 160 days. Then the system is again allowed to equilibrate during the period from 160 to 250 days. From 250 to 400 days, 100% quality steam at a temperature of 400 K is injected at a rate of 2 m^3 day^{-1} (cold water equivalent volume). Producing wells (constant pressure 20 kPa) were placed as shown in Figure 5.

Full details about the fluid properties, relative permeabilities and capillary pressures can be

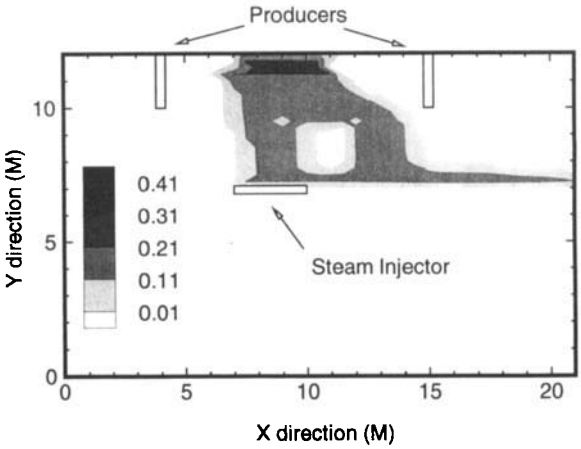

Figure 5. DNAPL contours, 2D example, time 250 days

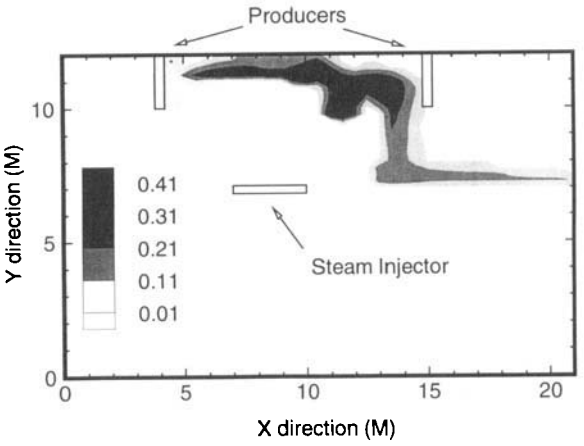

Figure 6. DNAPL contours, 2D example, time 254 days

found in Reference 13. This problem was computed on both 22 × 14 and 43 × 27 grids. Rectangles were divided into triangles as in Reference 21.

The NAPL saturation contours at 250 days are shown in Figure 5. Note that the heterogeneities have caused the DNAPL to spread out from the injection point as the DNAPL sinks through the water table. Observe that a finger of NAPL forms along the lower boundary owing to the ambient groundwater flow. Note also that a region of high NAPL saturation exists on the low-permeability shelf just below the injection point. This region is shielded from the steam injector by the low-permeability shelf.

Figures 6–9 show the NAPL saturations at various times during the steam injection (43 × 27 grid). At 400 days only a small amount of NAPL remains in the non-aqueous phase. Figure 10 shows the total amount of DNAPL injected and then produced through the production wells as a function of time for both 22 × 14 and 43 × 27 grids. The injection and equilibration phases can be seen in the straight lines from 50 to 160 days and from 160 to 250 days.

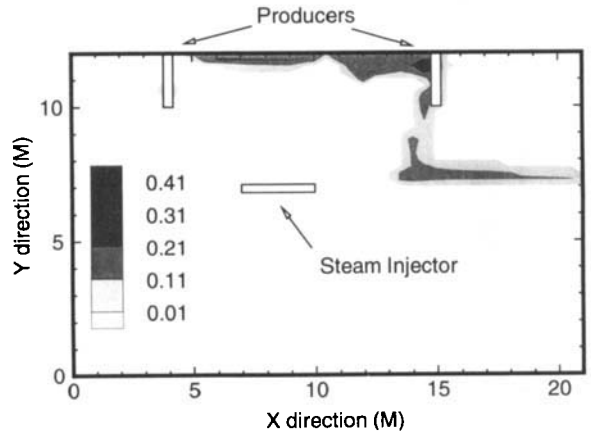

Figure 7. DNAPL contours, 2D example, time 257 days

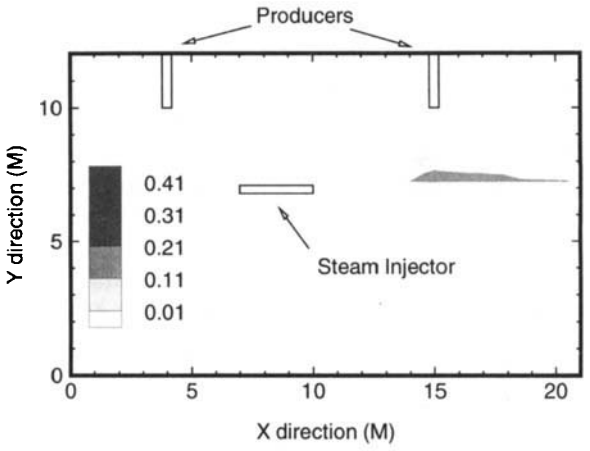

Figure 8. DNAPL contours, 2D example, time 267 days

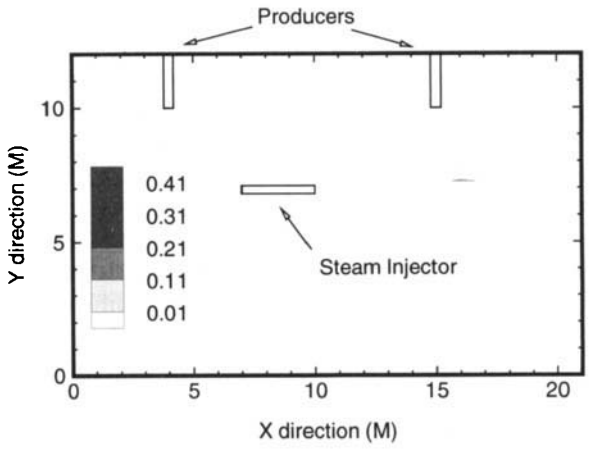

Figure 9. DNAPL contours, 2D example, time 400 days

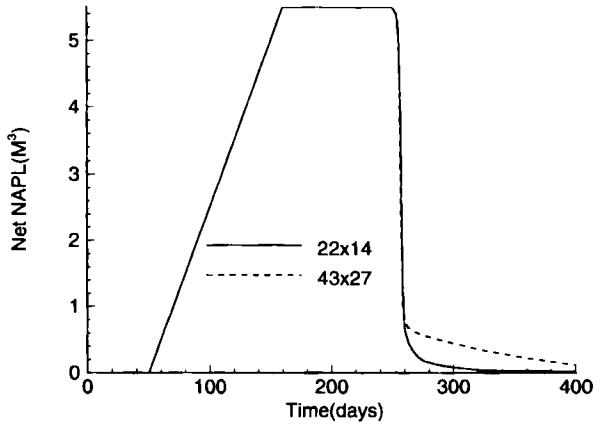

Figure 10. Volume of DNAPL (injected − produced) for 22 × 14 and 43 × 27 grids

Although the finer grid shows some difference in the DNAPL removal rate at the end of the recovery period, both computations result in removal of most of the mass of the DNAPL at the end of the steam injection period. Consequently, for the purposes of comparing different scenarios, the coarse 22 × 14 grid would appear to be adequate.

In fact, the discretization error is quite small considering that upstream weighting of the mole fractions will be used whenever condition (31) is violated. However, close examination of the NAPL recovery process reveals the following: once the NAPL phase is heated up and begins to vaporize, a finger of contaminant-rich gas phase flows from the contaminated zone into the production well. Along this finger the contaminant mole fraction is very slowly varying and hence little numerical smearing results. There is some numerical diffusion transverse to the flow, but this is slow compared with the large convective transport along the finger. The primary reason for the slower recovery for the fine grid simulation is that the gas fingers are smaller on the finer grid, so some NAPL zones are bypassed and take longer to heat up and vaporize (bypassed zones are heated by conductive heating).

10. THREE-DIMENSIONAL EXAMPLES

The two-dimensional problem of the last section was extended to three dimensions as shown in Figure 11. A 22 × 13 × 14 grid was used. Each brick was divided into six tetrahedra as discussed in Reference 22. Boundary conditions were similar to those used for the two-dimensional example, except that no flow boundaries were imposed on the $x = 0$ m and $x = 50$ m faces. The low-permeability layers near the water table were broken up in the third dimension. All fluid properties were as given in Reference 13.

Initially the systems was equilibrated for 50 days and the DNAPL was injected from 50 to 160 days. The injection rates were 0·1 m^3 day^{-1} of TCE and $0{\cdot}1^3$ day^{-1} of toluene. Equilibration was allowed during the period from 160 to 250 days. Three different steam injection scenarios were investigated.

Case 1 used the placement of horizontal injectors and vertical producers shown in Figure 12. Each producer was held at a constant 20 kPa pressure. Each steam injector injected a total of 2 m^3 day^{-1} (cold water equivalent) of 100% quality steam at 400 K. The wells were modelled using the methods of Section 6.

Case 2 is shown in Figure 13. In this case only one steam injector is used. Steam was injected at a rate of 2 m^3 day^{-1}, 100% quality, temperature 400 K. Consequently, this case injected only half the amount of steam as compared with Case 1. All production wells were held at 20 kPa pressure.

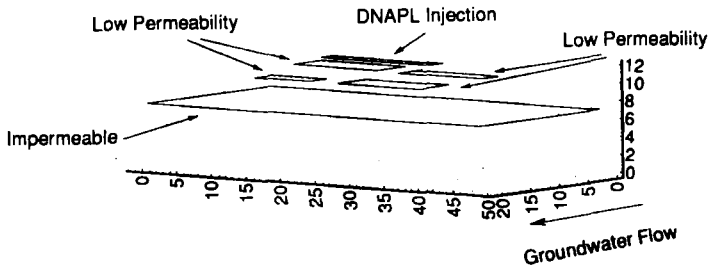

Figure 11. Problem configuration, 3D DNAPL steam injection

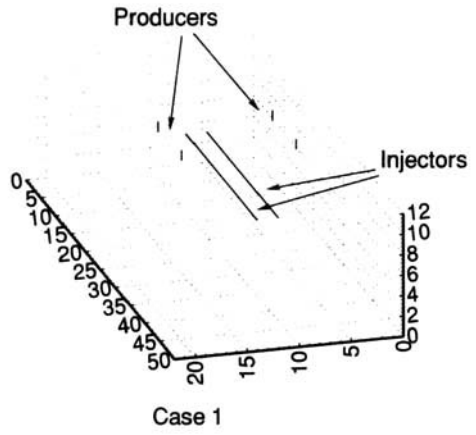

Figure 12. Injector–producer configuration, Case 1

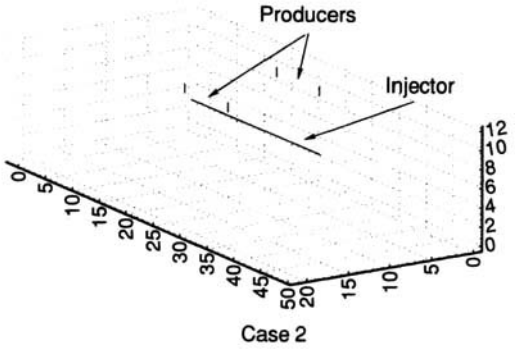

Figure 13. Injector–producer configuration, Case 2

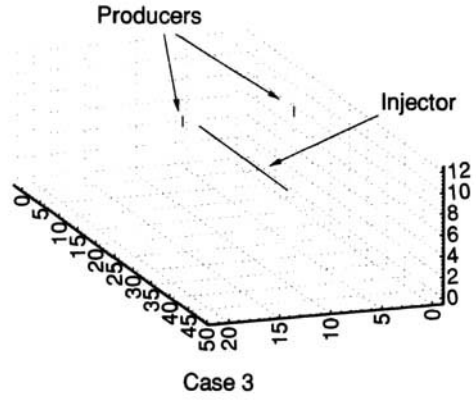

Figure 14. Injector–producer configuration, Case 3

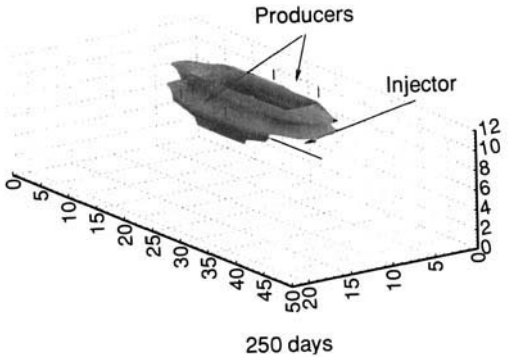

Figure 15. $S_n = 0{\cdot}01$ isosurface, 250 days, all cases

Case 3 is similar to Case 2, except that only two production wells (fixed pressure 20 kPa) were used. The placement of these wells is shown in Figure 14. The steam injection rate for Case 3 was as for Case 2.

Figure 15 shows the isosurface $S_n = 0{\cdot}01$ (the residual saturation in the NAPL–air system) at 250 days. Note that the top of the computational domain cuts the top of the isosurface. Figures 16–20 show $S_n = 0{\cdot}01$ isosurfaces at various times during the steam injection for Case 2. The NAPL contaminant gradually breaks up into smaller chunks, which then vaporize. The contaminant is then removed from the system by the production wells.

Figure 21 compares the total NAPL injected and produced through the production wells for all three cases. Although the rate of mass removal is different for all three cases, both Cases 1 and 2 remove most of the mass of contaminant by 400 days. This is rather surprising, since the steam injection rate for Case 2 is only half the steam injection rate for Case 1.

Case 3 has removed about 90% of the DNAPL by 400 days. If the injection period is extended, this case also removes >99% of the DNAPL. It is interesting to note that, at least for this example, poor placement of production wells has a bigger effect than lowering the steam injection rate.

Nevertheless, all three cases show good recovery of DNAPL. Recall that there are impervious layers which shield some of the DNAPL from the steam injector. Consequently, it would appear that steam injection is relatively insensitive to heterogeneities and injection/production well placement. This is in contrast with air sparging, which is quite sensitive to heterogeneities.[35] Conductive heating eventually causes vaporization of bypassed NAPL zones. This heated contaminant-rich gas eventually finds its way to the production wells via gravitational effects (hot gas will rise). Since in practice it is impossible to exactly characterize a remediation site, this insensitivity to heterogeneities would seem to make steam injection a good candidate process for remediation of DNAPL sites.

At the end of the steam injection for Cases 1 and 2, even though most of the mass of DNAPL has been removed, the mole fraction of contaminant in the water phase still exceeds drinking water standards. However, since there is no NAPL phase present, a water flush of this region (i.e. pump and treat) should quickly eliminate the remaining hazard. This is in contrast with traditional pump and treat methods, which must be continued for tens of years to remove DNAPLs if there is an NAPL phase present.

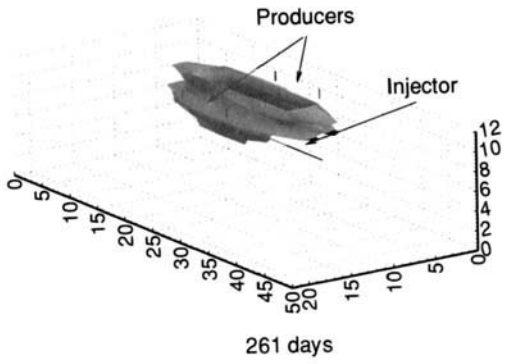

Figure 16. $S_n = 0{\cdot}01$ isosurface, 261 days, Case 2

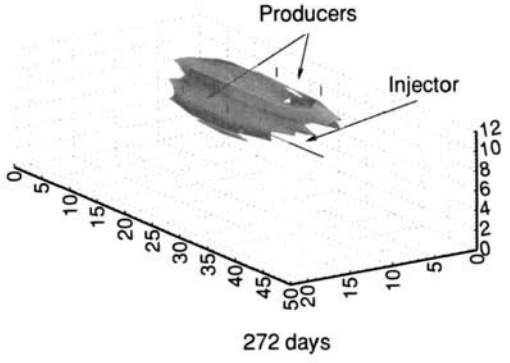

Figure 17. $S_n = 0{\cdot}01$ isosurface, 272 days, Case 2

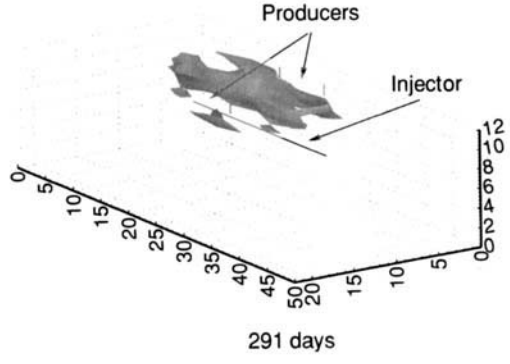

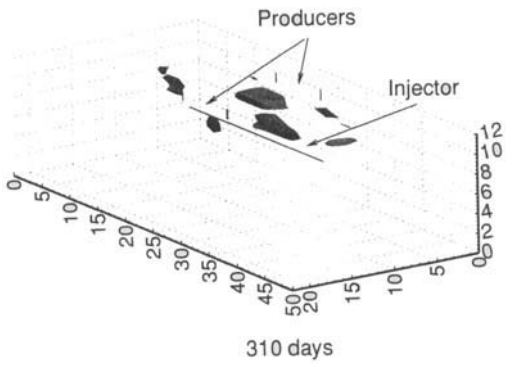

Figure 19. $S_n = 0{\cdot}01$ isosurface, 310 days, Case 2

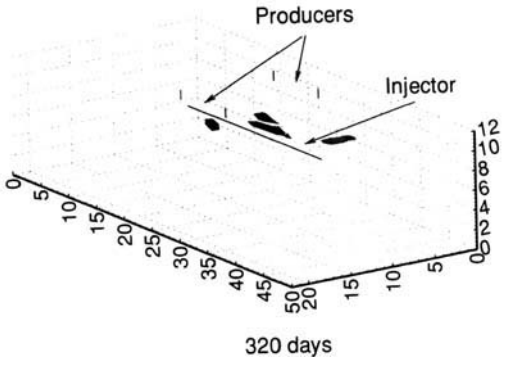

Figure 20. $S_n = 0{\cdot}01$ isosurface, 320 days, Case 2

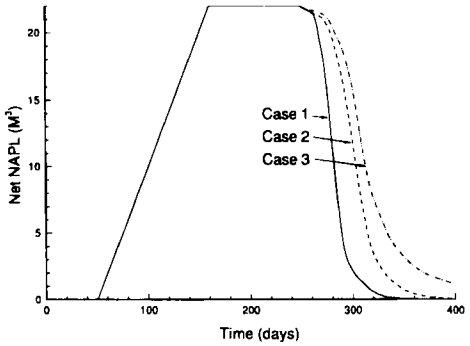

Figure 21. Volume of DNAPL (injected − produced) for all three cases, 3D steam injection scenarios

11. CONCLUSIONS

It is extremely important to ensure that the discretized algebraic equations for multicomponent, multiphase, non-isothermal subsurface flow converge to physically admissible solutions (i.e. positive mole fractions).[13] In regions where the flow is dominated by non-linear effects, single-point upstream weighting is a safe technique which helps to ensure convergence to physically reasonable solutions.[21] The two-dimensional grid refinement study suggests that single-point upstream for the non-linear terms is not overly diffusive. In regions where the contaminant transport is dominated by linear effects (i.e. no NAPL phase present), upstream weighting can certainly be overly diffusive. In these regions use of a non-linear flux limiter offers some improvement over single-point upstream weighting. However, it is necessary to be very cautious in the application of the flux limiter. Overly aggressive application of the flux limiter can cause the spurious appearance of small amounts of the NAPL phase and hence convergence problems.

Since the objective of this work was to investigate processes for the removal of the NAPL phase, which are highly non-linear phenomenan, the upstream weighting methods used here (single-point method in regions where $S_n > 0$, flux limiter in regions where $S_n = 0$) are probably adequate for practical purposes. This is because the actual mass of contaminant in the water and air phases is very small compared with the mass in the NAPL phase. However, if it is desired to use a single model for prediction of heat and mass transfer in the non-aqueous phase and for prediction of far-field plume evolution, other methods can probably be used. For example, if it is known that we are sufficiently far away from the NAPL source so that no NAPL phase can appear, then it may be possible to drop the requirement for strict monotonicity in the discretization, which would permit use of central weighting and higher-order time-stepping methods. Other possibilities are noted in Reference 44.

The choice of the primary variable set can have a large effect on the convergence of the Newton iteration. The simple variable set (25) (Method 1) is conceptually straightforward and works well for steam injection problems. However, in some cases this variable set performs poorly. For more general situations the more rigorous primary variable set (30) is probably preferable. For the primary variable set of Method 1 it is necessary to use the penalty source equation (29) to ensure convergence to the physically correct solution. Rather surprisingly, the penalty source was also necessary for good convergence of the primary variable set (30) (Method 2). It also appears that the penalty source enhances convergence of other choices of primary variables.[43]

The conceptually simple method of modelling multinode wells (i.e. horizontal wells) as a wellbore pseudonode worked very well for this application. This approach handles backflowing wells in a correct manner. The actual wellbore volume was used for the volume of the wellbore pseudonode. This caused no difficulty whatsoever.

In terms of simulation results it would appear that steam injection is relatively insensitive to heterogeneities and placement of injectors and producers compared with air sparging.[35] Of course, further tests with more complex heterogeneities are necessary to confirm this, but steam injection seems to be a promising approach for removing a large amount of contaminant mass from DNAPL sites. It remains to be seen as to whether this technique is economically feasible.

ACKNOWLEDGEMENTS

This work was supported by the National Sciences and Engineering Research Council of Canada, the Information Technology Research Center and the Waterloo Center for Groundwater

Research funded by the Province of Ontario. The author would also like to express his appreciation to HydroGeoLogic, Herndon, VA for hosting the author during a sabbatical visit.

REFERENCES

1. R. Falta, I. Javandel, K. Pruess and P. Witherspoon, 'Density driven flow of gas in the unsaturated zone due to evaporation of voltatile organic compounds', *Water Resources Res.*, **25**, 2159–2169 (1989).
2. B. Sleep and J. Sykes, 'Modelling of transport of volatile organics in variably saturated media', *Water Resources Res.*, **25**, 81–92 (1989).
3. P. C. Johnson, M. W. Kemblowski and J. D. Colthart, 'Quantitative analysis of the cleanup of hydrocarbon contaminated soils by in-situ soil venting', *Groundwater*, **28**, 413–429 (May 1990).
4. P. A. Forsyth and B. Y. Shao, 'Numerical simulation of gas venting for NAPL site remediation', *Adv. Water Res.*, **14**, 354–367 (1991).
5. D. A. Benson, D. Huntley and P. C. Johnson, 'Modelling vapor extraction and general transport in the presence of NAPL mixtures and nonideal conditions,' *Groundwater*, **31**, 437–445 (1993).
6. M. Sepher and Z. A. Samani, 'In situ soil remediation using vapor extraction wells, development and testing of a three dimensional finite difference model', *Groundwater*, **31**, 425–436 (1993).
7. K. S. Udell and L. D. Stewart, 'Field study of in situ steam injection and vacuum extraction for recovery of volatile organic solvents', *UCG-SEEHRL Rep. 89-2*, Berkely, CA, 1992.
8. H. B. Kerfoot, 'Subsurface partitioning of volatile organic compounds: effects of temperature and pore water content', *Groundwater*, **29**, 678–684 (1991).
9. R. Aines, 'Dynamic underground stripping demonstration project', *Res. Rep. UCRL-LR-105199-91*, Lawrence Livermore National Laboratory, Livermore, CA, 1991.
10. R. W. Falta, K. Pruess, I. Javandel and P. Witherspoon, 'Numerical modelling of steam injection for the removal of nonaqueous phase liquids from the subsurface 1. Numerical formulation', *Water Resources Res.*, **28**, 433–449 (1992).
11. R. W. Falta, K. Pruess, I. Javandel and P. Witherspoon, 'Numerical modelling of steam injection for the removal of nonaqueous phase liquids from the subsurface 2. Code validation and application', *Wate Resources Res.*, **28**, 451–465 (1992).
12. A. Adenekan and T. W. Patzek, 'Cleaning up spilled gasoline with steam: compositional simulations,' *SPE Paper 25257*, 1993.
13. P. A. Forsyth, 'A positively preserving method for simulation of steam injection for NAPL site remediation', *Adv. Water Res.*, **16**, 351–470 (1993).
14. K. Coats, 'In situ combustion model,' *Soc. Petrol. Eng. J.*, **20**, 533–554 (December 1980).
15. B. Rubin and W. Buchanan, 'A general purpose thermal model', *Soc. Petrol. Eng. J.*, **25**, 202–212 (April 1985).
16. M. Chien, H. Yardumian, E. Chung and W. Todd, 'The formulation of a thermal simulation model in a vectorized general purpose reservoir simulator', *SPE Paper 18418*, 1989.
17. R. Sharma, L. Nghiem, A. Siu, D. Collins and F. Mourits, 'Efficient modelling of wellbore backflow', *CIM Paper 92-16*, 1992.
18. L. S. Fung, A. Hiebert and L. X. Nghiem, 'Reservoir simulation with a control volume finite element method', *Soc. Petrol. Eng. J. Res. Eng.*, **7**, 349–357 (August 1992).
19. D. Collins, L. Nghiem, R. Sharma and Y. K. Li, 'Field scale simulation of horizontal wells', *J. Can. Petrol. Technol.*, **31**, 14–21 (1992).
20. F. X. Deimbacher and Z. E. Heinemann, 'Time dependent incorporation of locally irregular grids in large reservoir simulation models', *SPE Paper 25260*, 1993.
21. P. A. Forsyth, 'A control volume finite element approach to NAPL groundwater contamination', *SIAM J. Sci. Stat. Comput.*, **12**, 1029–1057 (1991).
22. F. W. Letniowski and P. A. Forsyth, 'A control volume finite element method for three dimensional NAPL groundwater contamination', *Int. j. numer. methods fluids*, **13**, 955–970 (1991).
23. P. A. Forsyth, 'Adaptive implicit criteria for two phase flow with gravity and capillary pressure', *SIAM J. Sci. Stat. Comput.*, **10**, 227–252 (1989).
24. B. van Leer, 'Towards the ultimate conservative difference scheme II. Monotonicity and conservation combined in a second order scheme', *J. Comput. Phys.*, **14**, 361-370 (1974).
25. P. K. Sweby, 'High resolution schemes using flux limiters for hyperbolic conservation laws,' *SIAM J. Numer. Anal.*, **21**, 995–1011 (1984).
26. M. Blunt and B. Rubin, 'Implicit flux limiting schemes for petroleum reservoir simulation', *J. Comput. Phys.*, **102**, 194–210 (1992).
27. H. Q. Yang and A. J. Przekwas, 'A comparative study of advanced shock capturing schemes applied to Burgers equation', *J. Comput. Phys.*, **102**, 139–159 (1992).
18. K. Aziz and A. Settari, *Petroleum Reservoir Simulation*, Academic, New York, 1979.
29. P. Huyakorn, S. Thompson and B. Thompson, 'Techniques for making finite element methods competitive in modelling flow in variably saturated porous media', *Water Resources Res.*, **20**, 1099–1115 (1984).

30. P. H. Sammon, 'An analysis of upstream weighting,' *Soc. Petrol. Eng. J. Res. Eng.*, **3**, 1053–1056 (1988).
31. G. A. Behie and P. A. Forsyth, 'Incomplete factorization methods for fully implicit simulation of enhanced oil recovery', *SIAM J. Sci. Stat. Comput.*, **5**, 543–561, (1984).
32. H. A. van der Vorst, 'Bi-CGSTAB: a fast and smoothly converging variant of Bi-CG for the solution of nonsymmetric linear systems,' *SIAM J. Sci. Stat. Comput.*, **13**, 631–645 (1992).
33. P. Arminjon and A. Dervieux, 'Construction of TVD-like artificial viscosities on two dimensional arbitrary FEM grids', *J. Comput. Phys.*, **106**, 176–198 (1993).
34. J. Goodman and R. J. LeVeque, 'On the accuracy of stable schemes for 2D conservation laws', *Math. Comput.*, **45**, 15–21 (1985).
35. A. Unger, *Ph. D. Thesis*, Department of Earth Sciences, University of Waterloo, in preparation.
36. B. Sleep and J. Sykes, 'Compositional simulation of groundwater contaminants by organic compounds 1. Model development and verification', *Water Resources Res.*, **29**, 1697–1708 (1993).
37. P. A. Forsyth, 'Radioactive waste disposal heating effects in unsaturated fractured rock,' *Numer. Heat Transfer A*, **17**, 29–51 (1990).
38. P. A. Forsyth, B. Rubin and P. K. W. Vinsome, 'The elimination of the constraint equation and modelling of problems with a non-condensible gas in steam simulation', *J. Can. Petrol. Technol.*, **20**, 63–68 (October 1981).
39. P. A. Forsyth and R. B. Simpson, 'A two phase, two component model for natural convection in a porous medium', *Int. j. numer. methods fluids*, **12**, 655–682 (1991).
40. P. A. Forsyth, Y. S. Wu and K. Pruess, 'Robust numerical methods for saturated–unsaturated flow with dry initial conditions in heterogeneous media,' *Adv. Water Resources Res.*, submitted.
41. D. W. Peaceman, 'Numerical interpretation of well-block pressures in numerical reservoir simulation with nonsquare grid blocks and anisotropic permeability', *Soc. Petrol. Eng. J.*, 531–543 (June 1983).
42. D. W. Peaceman, 'Interpretation of wellblock pressures in numerical reservoir simulation: Part III—Off center and multiple wells within a wellblock', *Soc. Petrol. Eng. J. Res. Eng.*, **5**, 227–232 (May 1990).
43. S. Panday, 'A comprehensive simulator for multiphase fluid flow and chemical transport in porous media', *NSF Final Rep. 92-61292*, prepared by HydroGeoLogic Inc., 1993.
44. C. Y. Chiang, M. F. Wheeler and P. B. Bedient, 'A modified method of characteristic technique and mixed finite elements for simulation of groundwater solute transport', *Water Resources Res.*, **25**, 1541–1549 (1989).